ZnO Hierarchical Micro/Nanoarchitectures: Solvothermal Synthesis and Structurally Enhanced Photocatalytic Performance*

By *Fang Lu, Weiping Cai,* and *Yugang Zhang*

A novel ZnO hierarchical micro/nanoarchitecture is fabricated by a facile solvothermal approach in an aqueous solution of ethylenediamine (EDA). This complex architecture is of a core/shell structure, composed of dense nanosheet-built networks that stand on a hexagonal-pyramid-like microcrystal (core part). The ZnO hexagonal micropyramid has external surfaces that consist of a basal plane $(000\bar{1})$ and lateral planes $\{0\bar{1}11\}$. The nanosheets are a uniform thickness of about 10 nm and have a single-crystal structure with sheet-planar surfaces as $\{2\bar{1}\bar{1}0\}$ planes. These nanosheets interlace and overlap each other with an angle of $60°$ or $120°$, and assemble into a discernible net- or grid-like morphology (about 100 nm in grid-size) on the micropyramid, which shows a high specific surface area ($185.6\,\mathrm{m^2\,g^{-1}}$). Such a ZnO micro/nanoarchitecture is new in the family of ZnO nanostructures. Its formation depends on the concentration of the EDA solution as well as on the type of zinc source. A two-step sequential growth model is proposed based on observations from a time-dependent morphology evolution process. Importantly, such structured ZnO has shown a strong structure-induced enhancement of photocatalytic performance and has exhibited a much better photocatalytic property and durability for the photodegradation of methyl orange than that of other nanostructured ZnO, such as the powders of nanoparticles, nanosheets, and nanoneedles. This is mainly attributed to its higher surface-to-volume ratio and stability against aggregation. This work not only gives insight into understanding the hierarchical growth behaviour of complex ZnO micro/nanoarchitectures in a solution-phase synthetic system, but also provides an efficient route to enhance the photocatalytic performance of ZnO, which could also be extended to other catalysts, such as the inherently excellent TiO_2, if they are of the same hierarchical micro/nanoarchitecture with an open and porous nanostructured surface layer.

1. Introduction

Zinc oxide (ZnO), an important II–VI semiconductor with a bandgap of 3.37 eV and a large exciton binding energy of 60 meV, has been extensively studied because of its potential applications in solar cells,[1] sensors,[2,3] photocatalysis,[4] etc. Over the past few years, tremendous efforts have been made to synthesize diverse nanometer-scaled ZnO building blocks (e.g., nanoparticles, nanowires, nanobelts, nanotubes, and nanosheets) with controlled sizes and morphologies.[5–8] Recently, hierarchical and complex ZnO micro/nanoarchitectures have stimulated much attention since such architectures combine the features of micrometer- and nanometer-scaled building blocks and show unique properties different from

those of the mono-morphological structures.[9] Many micro/nanocomposite ZnO architectures, such as bridge and nails,[10] propellers,[11] and microcrystals, nanocavities, nanowalls, and nanorods,[12] have been synthesized by gas-phase reactions. Alternatively, two main solution-based routes have also been developed to fabricate various hierarchical micro/nanostructured ZnO. Such routes are attractive because of their mild synthetic conditions, low-cost, and mass production. Both solution-based routes involve a multi-step process. One is a precursor-induced synthesis, in which the low solubility of the pre-synthesized precursor in the reaction solvent induces a controlled release of Zn^{2+} ions favorable for ZnO hierarchical growth. For example, ZnO hierarchical structures with ring-like nanosheets that stand on spindle-like rods were synthesized from a flake-like precursor $Zn_5(OH)_8Cl_2\cdot2H_2O$.[13] Flower-like cupped-end ZnO micro-rod bundles were hydrothermally synthesized from a sheet-shaped precursor $ZnCl_2(N_2H_4)_2$ heated at $140\,°C$ for 12 h.[14] Hierarchical nanostructured ZnO with a bladed bundle-like architecture was fabricated from a flower-like precursor $ZnO\cdot0.33ZnBr_2\cdot1.74H_2O$.[15] The other route is a sequential nucleation and growth route, by which the oriented primary ZnO rods, the secondary needle-like nanobranches (or nanoplates), and the tertiary nanoplates (or nanobranches) are synthesized stepwise on specific sites of previous structures.[16,17] Both the size and morphology have a significant influence on the

[*] Prof. W. P. Cai, Dr. F. Lu, Y. G. Zhang
Key Laboratory of Materials Physics
Anhui Key Lab of Nanomaterials and Nanotechnology
Institute of Solid State Physics, Chinese Academy of Sciences
Hefei 230031 (P. R. China)
E-mail: wpcai@issp.ac.cn

FULL PAPER

properties of the semiconductor oxides. New properties and promising applications in many fields may be induced from the unique structures. However, fabrication of more complex ZnO micro/nanoarchitectures in one step is still a significant challenge.

An important application of ZnO is as a photocatalyst in environmental protection. Through the photocatalytic generation of hydrogen peroxide,[18] ZnO can be utilized for the degradation of organic pollutants in nearly neutral solution, and for the sterilization of bacteria and viruses.[19] Recently, semiconductor photocatalysts on a nanometer-scale have become more and more attractive because of their different physical and chemical properties from bulk materials.[20] Since the photocatalytic reaction occurs at surfaces, a nanosized semiconductor will increase the decomposition rate because of the increased surface area. However, it should be mentioned that nanometer-scaled building blocks (such as nanoparticles, nanorods, and nanosheets) with a high surface-to-volume ratio tend to aggregate during aging, which results in the unwanted reduction in the active surface area. An available way to prevent the particles from aggregation is to immobilize the photocatalysts in the form of a thin film on a substrate.[20] In this case, however, the efficiency is significantly lower than that of the corresponding suspensions. Therefore, the synthesis of novel nanostructured ZnO that is stable against aggregation and possesses a higher surface-to-volume ratio, is still one of the most important tasks for its environmental remediation applications.

In this article, a newly structured ZnO hierarchical micro/nanoarchitecture is reported that has been synthesized by a facile solvothermal approach in an aqueous solution of ethylenediamine (EDA, $NH_2CH_2CH_2NH_2$) without self-assembled templates or matrixes. It is composed of microsized conic-like particles, which are built by many alternating nanosheets with a thickness of 10 nm as a highly branched nanoarchitecture standing on hexagonal-pyramid-like core microcrystals. Such ZnO structures show a high surface-to-volume ratio and stability against aggregation. Importantly, the ZnO shows a strong structure-induced enhancement of photocatalytic performance and exhibits a significantly improved photocatalytic property and durability in the photodegradation of methyl orange (MeOr) than that of other nanostructured ZnO, such as the powders of nanoparticles, nanosheets, and nanoneedles. This work not only gives insight into understanding the hierarchical growth behaviour of complex ZnO micro/nanoarchitectures in a solution-phase synthetic system, but also provides a new way to improve the photocatalytic performance by designing a desirable micro/nanoarchitecture. Such a structure-induced enhancement of photocatalytic performance could also be applicable to the other catalysts, such as the inherently excellent TiO_2, and other kinds of hierarchical micro/nanoarchitectures with open and porous nanostructural surface layers.

In this work, the aqueous solution of EDA was prepared with deionized water with a 1 : 7 volume ratio. A piece of zinc foil was placed into the solution together with a small amount

of NaOH before reaction in an autoclave at 160 °C. The products on the Zn foil were then taken out, rinsed, and dried for 12 h (see Experiment section for details).

2. Results and Discussion

2.1. Morphology and Structure

An X-ray diffraction (XRD) pattern of the as-synthesized products scraped off from the Zn foil is shown in Figure 1, in which the diffraction of standard hexagonal (wurtzite) ZnO powders is also included (JCPDS No. 36-1451). Obviously, all the diffraction peaks can be indexed to the wurtzite ZnO.

Figure 2 demonstrates the corresponding morphology of the as-synthesized ZnO. The products consist of a large number of conical-like microsized particles (see Fig. 2A). A high-magnification field emission scanning electron microscopy (FESEM) image shows that the conicals are of a net- or grid-like morphology (see Fig. 2B). They seem to be built of numerous nanosheets that almost stand vertically on the conical's surface and alternately connect with each other to form networks or grids. The ZnO nanosheets are about 10 nm in thickness and hundreds of nanometers in planar size, as shown in Figure 2C. Close examination of these nanosheet-built networks reveals that there is nearly a 60° angle between adjacent connected nanosheets, for many of the nanosheets, and they are about 100 nm in grid-size. A slight deviation from 60° should mainly be attributed to the tilted observation and the distortion because of the jostle among the densely arranged nanosheets (see the arrow-marks in Fig. 2C). At some regions of incomplete nanosheet-built networks, where jostle exists relatively weakly, more adjacent nanosheets are easily observed joining each other with the regular angles of about 60° (as shown in Fig. 2D).

Figure 3A presents a transmission electronic microscopy (TEM) image for a typical isolated ZnO nanosheet obtained by
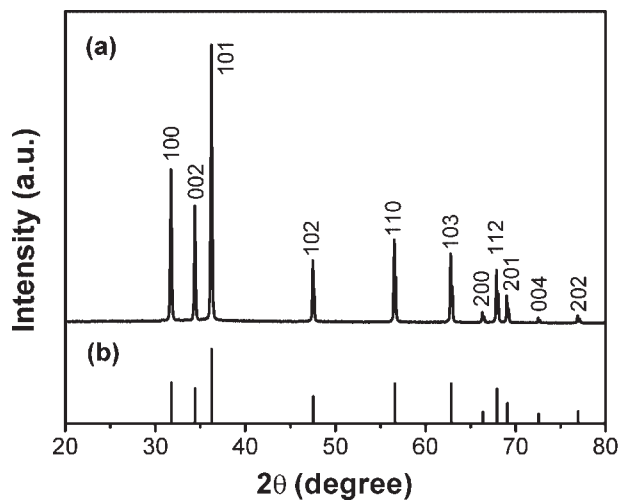

Figure 1. XRD patterns of as-prepared products (a) and standard ZnO (JCPDS no. 36-1451) (b). Marked indices correspond to planes of ZnO.
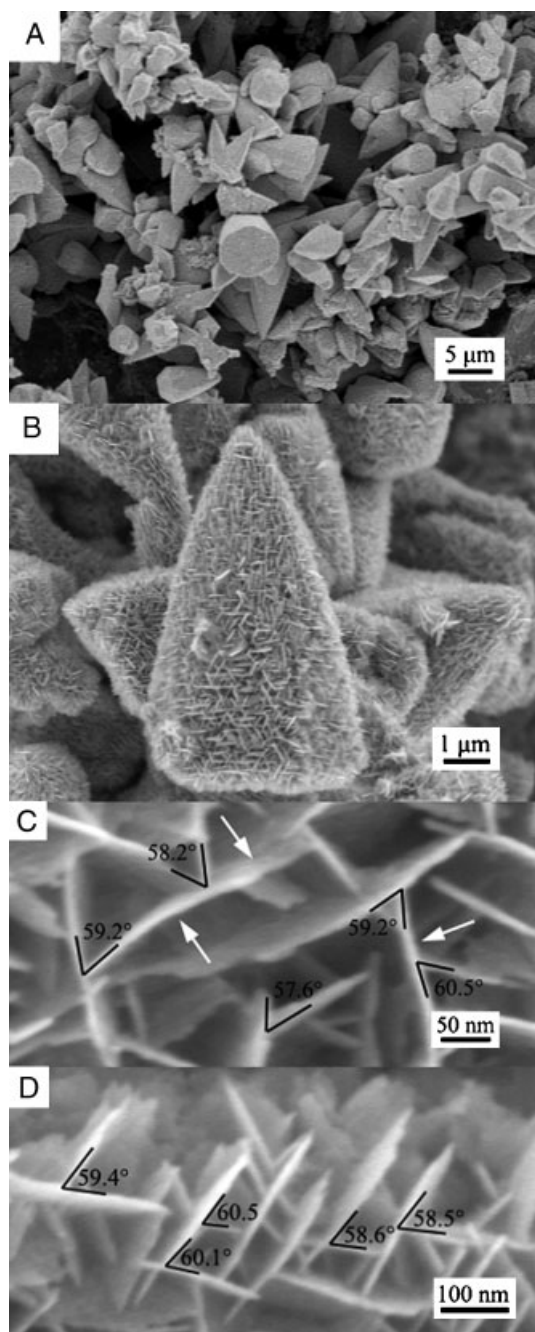
Figure 2. FESEM images of the products prepared by the solvothermal reaction at 160 °C for 12 h, $V_{DIW}/V_{EDA} = 1:7$. A) A general-view image of the products. B) The local magnification image of (A). C) A further enlarged top-view image of (B). D) Enlarged local image at the edge of the networks, incomplete nanosheet-built networks. The arrows in (C) indicate the distortion that results from the jostle action between the densely arranged nanosheets.

Figure 3. A) TEM image of a typical nanosheet from the as-prepared sample (inset: SEAD pattern corresponding to the small frame area marked in the nanosheet, recorded along the [$2\bar{1}\bar{1}0$] zone), and B) the corresponding high-resolution TEM image. The arrow marked at the one end of the nanosheet indicates an interface disconnected from another sheet.

ultrasonic dispersion of the as-prepared sample in ethanol. The corresponding selective area electron diffraction (SAED) pattern (the inset in Fig. 3A) indicates the single crystalline nature of the isolated nanosheet. The high-resolution TEM
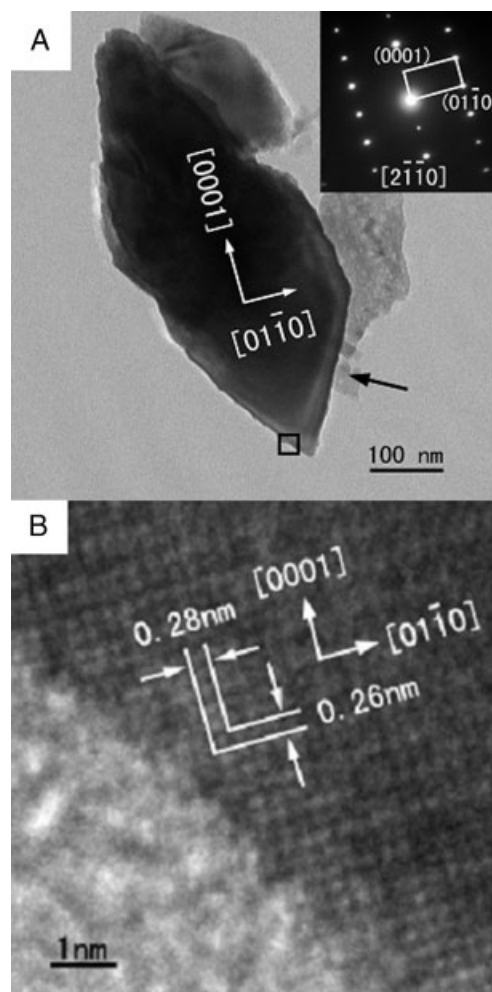
image exhibits well-resolved two-dimensional lattice fringes with the spacings of 2.6 and 2.8 Å, which are in good agreement with the interplanar spacings of {0002} and {$01\bar{1}0$} planes respectively, as shown in Fig. 3B. It indicates that the nanosheet is of single-crystal structure with sheet-planar surfaces {$2\bar{1}\bar{1}0$}. One end of the nanosheet, marked by an arrow in Figure 3A, seems to be an interface disconnected from another sheet.

Full nitrogen sorption isotherms were measured to gain information about specific surface area and the pore size of such structured ZnO powders, as shown in Figure 4A. The adsorption curve is of a reverse 'S'-shape, which is a normal physical adsorption isotherm. It means that a molecular monolayer is first formed in the low pressure region (below the pressure at point *O* or inset of Fig. 4A). The specific surface area was thus evaluated to be 185.6 m^2 g^{-1} from data points in
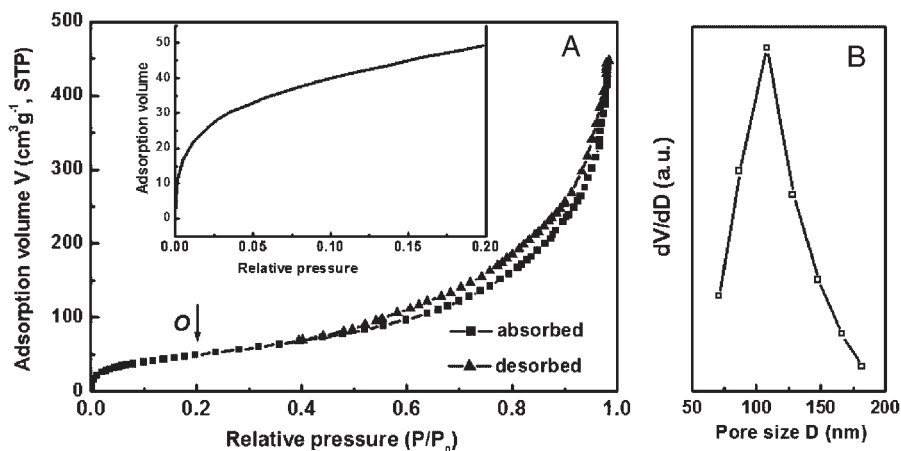
Figure 4. Full nitrogen sorption isotherms (A) and pore size distribution (B) of the as-prepared sample. The inset in (A) is an enlarged curve below the reduced pressure 0.2. Adsorption volume V is in cm^3 g^{-1} at standard temperature pressure (STP).

tion process was examined by FESEM. Figure 5 shows the morphologies of the sample after different reaction times. After reaction for 1 h, no ZnO structures with a discernable morphology are formed on the surface of the zinc foil, as shown in Figure 5A. After 2 h, a few hexagonal prism-like microcrystals with a pyramidal top are observed, which aggregate together on the substrate (see the arrow marks), as shown in Figure 5B. The surfaces of these crystals are clean and there is nothing covering them (see the inset in Fig. 5B). After 4 h reaction time, some small sheets are found to stand nearly vertically on the surface of the micro-sized hexagonal pyramids, as shown in
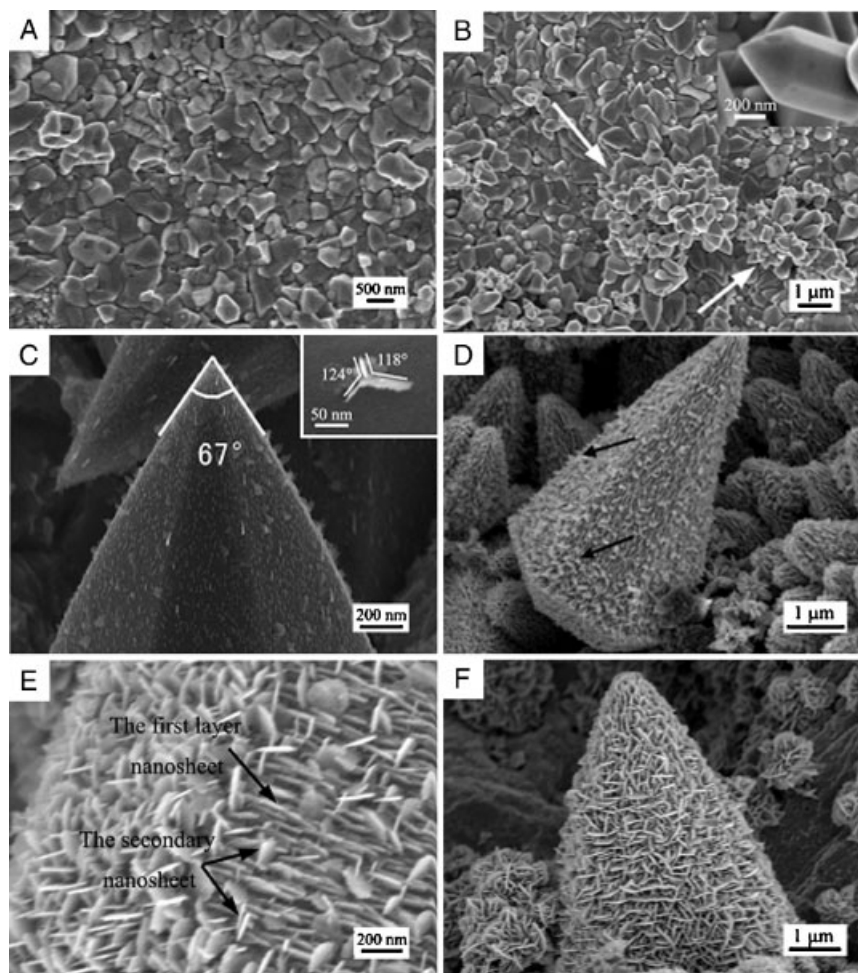
this pressure range by the Brunauer–Emmett–Teller (BET) equation.[21] A further increase of the pressure leads to multilayer adsorption. When the pressure is quite high (or the reduced pressure $x > 0.5$), the adsorption volume (in cm^3 g^{-1} at standard temperature and pressure, i.e., STP) increases sharply and the desorption hysteresis occurs in the reduced pressure range from 0.5 to 0.98 (see Fig. 4A), which indicates the occurrence of the condensation of nitrogen in the pores within this pressure range. Based on the cylindrical-shaped approximation of pores as usually taken, the pore size distribution of the sample can be obtained (the results are supplied by the sorption apparatus), as shown in Figure 4B. Most of the pores fall into the size range of 70 to 150 nm and peaks around 108 nm, which is in agreement with the results of the FESEM analysis (see Fig. 2). Obviously, this hierarchically structured ZnO with high specific surface area will be stabile against aggregation, and may exhibit potential application in catalysis and sensing (see the following text).

2.2. Morphology Evolution with Reaction Time

To understand how the ZnO hierarchical structures are formed, the time-dependent morphological evolu-

Figure 5. FESEM images of the samples after different reaction times at 160 °C for the solution with $V_{DIW}/V_{EDA} = 1$: 7 and Zn foil. A) 1 h, B) 2 h, C) 4 h, D,E) 8 h, and F) 16 h. The inset in (C) is a local top view, which exhibits that partial nanosheets are connected in every three sheets, with the angle between two adjacent sheets is about 120°. The arrows in (D) indicate that the outmost blade-like nanosheets stand astride on the bottom rows.

Figure 5C. The angle between two opposite edges at the tip of the micropyramid measures about 67°, which is close to the angle between two opposite edges at the tip of the hexagonal pyramid composed of the $\{0\bar{1}11\}$ planes as the side surfaces (63.94°). The deviation could result from a slightly tilted view of the shooting angle. The local high-magnification FESEM image (the inset in Fig. 5C) exhibits that partial sheets have been connected, in every three sheets, with the angle between two adjacent sheets near 120°. When the reaction is prolonged further, a significant change occurs in the morphology of the ZnO microcrystals. They evolve from micropyramids into more a complex micro/nanoarchitecture with a delicate surface structure. After 8 h, all the surfaces of the micropyramids become rougher, as displayed in Figure 5D. Two layers of vertically arranged nanosheets seem to be formed on the surface of the micropyramids. The top layer is incomplete (see the arrow-marked areas in Fig. 5D). Two such layers of

vertically arranged nanosheets can be seen more clearly in Figure 5E, which corresponds to the local area of Figure 5D. Most of the nanosheets on the surface of the pyramid-like microcrystal (or the first layer) are arranged into a dense parallel row (non-network pattern), while the nanosheets on the top layer stand vertically and show a net-like morphology from the top view (see Fig. 5E), which is similar to that shown in Figure 2. When the reaction time is up to 12 h, a complete top layer is formed with the nanosheets nearly vertically standing and interlacing into a net-like structure, as shown in Figure 2. The whole hierarchically structured particles exhibit a net- or grid-like surface morphology. If the reaction time further increases to 16 h, the product still shows a similar morphology but has grown larger in size since more layers are formed, as seen in Figure 5F.

Figure 6A presents a TEM image for a typical isolated ZnO nanosheet from the sample shown in Figure 5D. This sheet exhibits a similar shape to that of nanosheets in the bottom layer shown in Figure 5E. One end of the nanosheet, marked by an arrow in Figure 6A, seems to be an interface disconnected from the micropyramid's surface. The SAED pattern (the inset in Fig. 6A) and high-resolution TEM examination (Fig. 6B) confirm it's single crystalline nature. The angle between the end plane and the known crystal plane ($01\bar{1}0$) can be measured from the image to be about 27° (see Fig. 6A), which is close to the interplanar angle between the ($01\bar{1}0$) and ($01\bar{1}1$) planes (28.4°). Thus the end plane of the nanosheet marked by an arrow in Figure 6A can be determined to be the crystal plane $\{01\bar{1}1\}$. Such results are helpful to understand the growth mechanism of the ZnO hierarchical structures observed here.
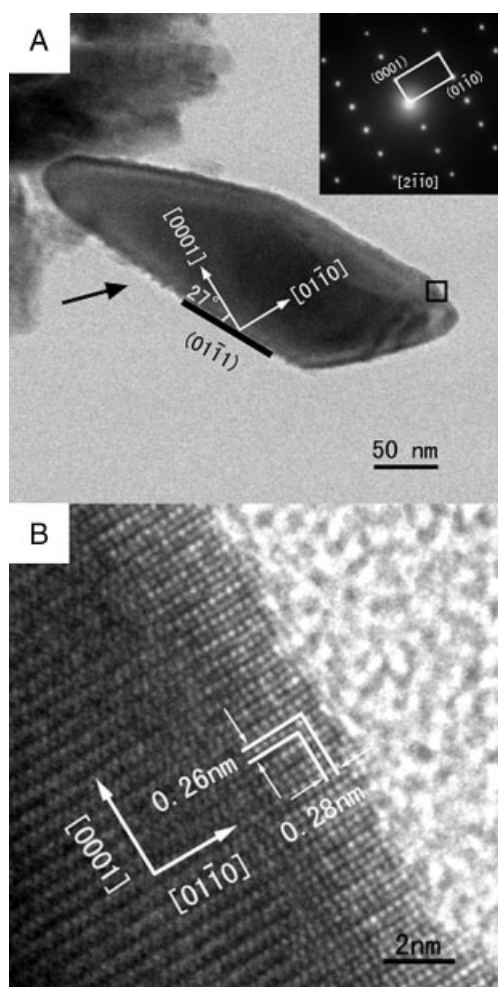

Figure 6. A) TEM image of a typical nanosheet from the sample shown in Figure 5D (inset: the SEAD pattern that corresponds to the small frame area marked in the nanosheet, recorded along the $[2\bar{1}\bar{1}0]$ zone), and B) the corresponding high-resolution TEM image. The arrow marked at the one end of the nanosheet indicates an interface disconnected from the micropyramid's surface.

2.3. Influencing Factors

Further experiments indicate that the concentration of the EDA solution is crucial for the formation of such complex ZnO hierarchical structures. Figure 7 exhibits the morphologies of the products obtained from the aqueous solution of EDA prepared by different volume ratios of deionized water to EDA (V_{DIW}/V_{EDA}) when keeping other experimental conditions unchanged. In the absence of water, only nearly vertically arranged nanorod arrays are formed on the Zn foil in pure EDA (Fig. 7A). The diameters of the nanorods fall into the range between 50 and 200 nm. When the ratio of V_{DIW}/V_{EDA} is increased to about 3: 37, the products consist of conical-like microparticles with a rough surface, as illustrated in Figure 7B. Further examination shows that there are many vertically standing nanoplatelets on the surface (see inset 1 in Fig. 7B, a local side view). These nanoobjects do not arrange in a net-like pattern. Nevertheless, some adjacent connected nanoplatelets assume a regular angle of 60° (see inset 2 in Fig. 7B, a local top view). A further increase in V_{DIW}/V_{EDA} to 1: 7 gives rise to a hierarchical structure with a surface grid-like morphology, as shown in Figure 2. However, if V_{DIW}/V_{EDA} is too high (say, 1: 3), randomly distributed microrods are observed on the Zn foil
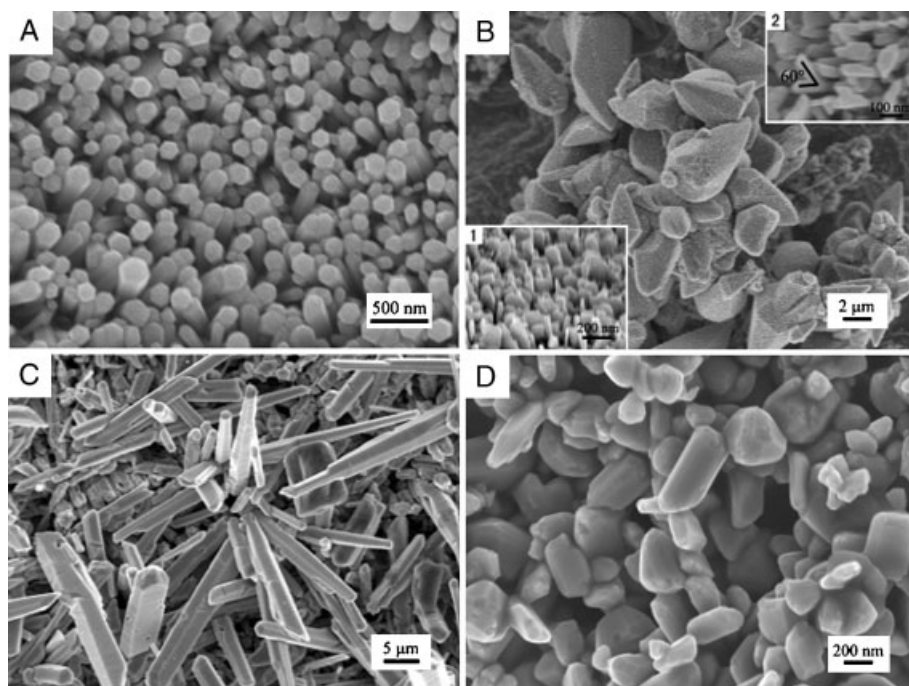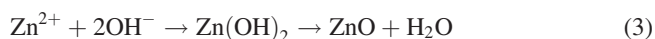
Figure 7. FESEM images of the products synthesized from the reaction solution with Zn foil and different V_{DIW}/V_{EDA} at 160 °C for 12 h. A) 0, B) 3: 37, and C) 1: 3 (the insets 1 and 2 are, respectively, a side view and a top view for the local area on the surface of a microconical). D) The FESEM image of the products prepared with $Zn(NO_3)_2$ instead of Zn foil at 160 °C for 12 h ($V_{DIW}/V_{EDA} = 1: 7$).

where m is a positive integer. In a basic environment with EDA, Zn atoms at the liquid–solid (Zn foil) interface are oxidized to form the soluble coordinated ions $[Zn(EDA)_m]^{2+}$, which further decompose into Zn^{2+} ions at an elevated temperature (>90 °C) according to Reactions (1) and (2).[22,23] The Zn^{2+} ions will further form $Zn(OH)_2$ with OH^-. Finally, ZnO is obtained by decomposition of $Zn(OH)_2$ (Reaction (3)). When the concentration of ZnO has reached supersaturation, ZnO crystal nuclei form and then grow according to the growth habit of ZnO crystals.

From the results of the reaction-time dependent morphology, it is known that the growth of the ZnO hierarchical architectures can be described in two steps, as illustrated in Figure 8. During the first stage, ZnO hexagonal pyramid-like microcrystals are formed after nucleation. Generally, the faces perpendicular to the fast direction of growth have smaller surface areas, and the faces, whose normal directions correspond to slow growing ones, thus dominate the final morphology. For the ZnO crystal, the growth rates V along the normal directions of different low-index planes in alkaline medium are described as follows: $V_{(0001)} > V_{(10\bar{1}0)} \geq V_{(10\bar{1}\bar{1})} > V_{(10\bar{1}1)} > V_{(000\bar{1})}$.[24] In our case, the Zn foil and the mixture solution are used to control the release rate of Zn^{2+}. While the reaction proceeds, the surfaces whose normal directions are of fast growth rate disappear while the slow growing surfaces remain. As a result, ZnO hexagonal pyramid-like microcrystals with a $(000\bar{1})$ basal plane and $\{0\bar{1}11\}$ lateral planes are formed (as shown in Fig. 5B or schematically illustrated in Fig. 8A). This is different from the growth mechanism of the tubular graphite cones obtained by a chemical vapor deposition method reported by Zhang et al.,[25] which consist of coaxial tubular graphite sheets. In that case, the cone-shaped structure is caused by a gradual shortening of the length of the graphite sheets along the axial direction from the inner to the outer layers of the tube, and layer steps are present on the cone surface.

The second step is the formation of nanosheet networks on the facets of the pre-formed ZnO microcrystals. After the hexagonal pyramid-like microcrystals are formed, further growth will be difficult because of the pyramid-like geometry. However, there exist inevitable defects or bulges on the lateral planes of the microcrystals. Such bulges will preferentially grow along the $\langle 0001 \rangle$ and $\langle 01\bar{1}0 \rangle$ directions (both are the fast growth directions) within the $\{2\bar{1}\bar{1}0\}$ plane and form nanosheets nearly vertically standing on the lateral surface

(see Fig. 7C). These results indicate that products only with a single morphology, rather than hierarchical structures, are formed in an EDA aqueous solution with too low or too high a percentage of deionized water. As such, ZnO hierarchical architectures can only be synthesized in a binary solution with a suitable ratio of V_{DIW}/V_{EDA} (about 1: 7).

In addition, the choice of zinc source in the reaction system also shows an obvious influence on the formation of the ZnO hierarchical structure. Zinc salts, such as $Zn(NO_3)_2$, have been used instead of zinc foil as the starting material while keeping all other conditions unchanged. When $Zn(NO_3)_2$ is used as the reactant, ZnO particles with an irregular shape ($\sim$100–500 nm in size) are obtained and no hierarchical structures are formed (Fig. 7D).

2.4. Formation of the ZnO Micro/Nanoarchitecture

When the precursor solution is heated, reactions can occur as follows:[22,23]

$$Zn + mEDA + 2H_2O \rightarrow [Zn(EDA)_m](OH)_2 + H_2 \qquad (1)$$

$$[Zn(EDA)_m]^{2+} \leftrightarrow Zn^{2+} + mEDA \qquad (2)$$

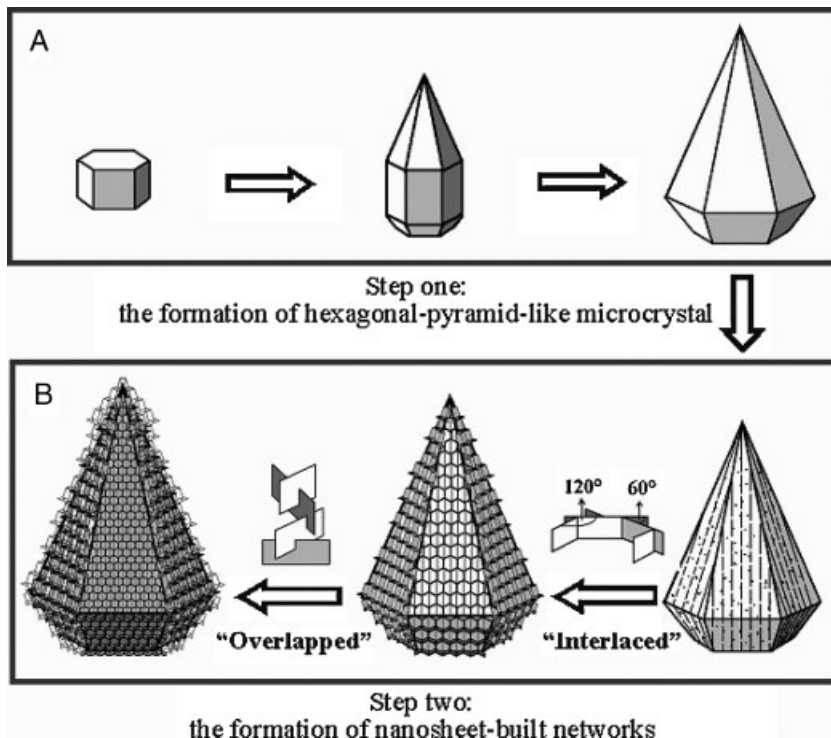$$Zn^{2+} + 2OH^- \rightarrow Zn(OH)_2 \rightarrow ZnO + H_2O \qquad (3)$$

Figure 8. The schematic illustration of a two-step sequential growth model for the formation of the micro/nanoarchitectured ZnO.

Fig. 8B). This growth process is similar to that of α-MnO$_2$ hierarchical structures reported by Xie et al.[26] and the Pt 'sea urchin' reported by Xia et al.[27] Finally, combining the TEM examinations shown in Figure 3 and 6, and based on the discussion above, the orientation relationship in this ZnO micro/nanohierarchical architecture can be schematically summarized in Figure 9.

Obviously, the formation of such a hierarchical structure should depend on the growth rate of the ZnO crystal or the release rate of Zn^{2+} ions into the solution. Too high and low a growth rate of the crystal, which corresponds to the release rate of Zn^{2+} ions in Reaction (1), would be unbeneficial to the two-step growth mentioned above. A high growth rate can only lead to single morphology particles (one-step growth) and a low growth rate would result in quasi-equilibrium growth. When V_{DIW}/V_{EDA} is low or no water is added to the solution, the release rate of Zn^{2+} ions into the solution, and hence the growth rate, would be slow according to Reaction (1). In this case, quasi-equilibrium growth of ZnO will occur, which leads to the formation of nearly vertically arranged nanorod arrays on the Zn foil (see Fig. 7A). Contrarily, a high ratio of V_{DIW}/V_{EDA}, or the use of Zn(NO$_3$)$_2$ instead of Zn foil, will induce a high release rate of Zn^{2+} ions and hence fast growth of crystals, which leads to randomly distributed particles with a single morphology (see Figs. 7C and 7D). The formation of ZnO hierarchical structures or the two-step growth mode can only occur for a certain release rate of Zn^{2+} ions (here, using Zn foil as zinc source and the ratio of $V_{DIW}/V_{EDA} = 3:37$ to 1:7), which provides a kinetically favorable condition for ZnO hierarchical growth and is similar to the precursor-induced synthesis of hierarchical nanostructured ZnO.[13–15]
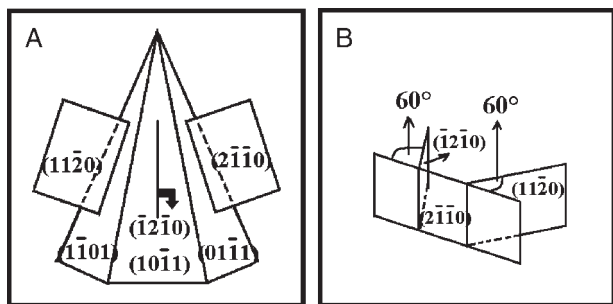
of the microcrystals. In addition, there also inevitably exist some outshoots on the growing nanosheets. Such outshoots will grow and lead to the formation of secondary dendrite-like (or branched) nanosheets with terminated $\{2\bar{1}\bar{1}0\}$ facets and interplanar angles (60°) for the same reason. In addition, third or fourth branched nanosheets could be formed on the as-grown nanosheets. Finally, more and more nanosheets with a $\{2\bar{1}\bar{1}0\}$ planar surface, which interlace and overlap with each other into a discernible multilayer and network structure, stand on the microcrystals, and constitute the ZnO hierarchical micro/nanoarchitecture (see Fig. 2 or schematic illustration in

Figure 9. Schematic drawings of orientation relationship in ZnO hierarchical growth. A) The primary hexagonal micropyramid covered with the nanosheets and B) some secondary or tertiary nanosheets grown from the sheet-planar surfaces of the one formed previously.

2.5. Photocatalytic Activity

It is well known that ZnO has been used as a semiconductor photocatalyst for the photoreductive dehalogenation of halogenated benzene derivatives, the photocatalytic degradation of water pollutants, and the photocatalytic reduction of toxic metal ions. Obviously, the as-synthesized ZnO micro/nanoarchitecture with open and porous nanostructural surface layers presented here should show a higher photocatalytic activity because of its special structure, which exhibits a high specific surface area ($>180\,m^2\,g^{-1}$) and stability against aggregation. This structure-induced enhancement of photocatalytic performance has been confirmed by further experiments.
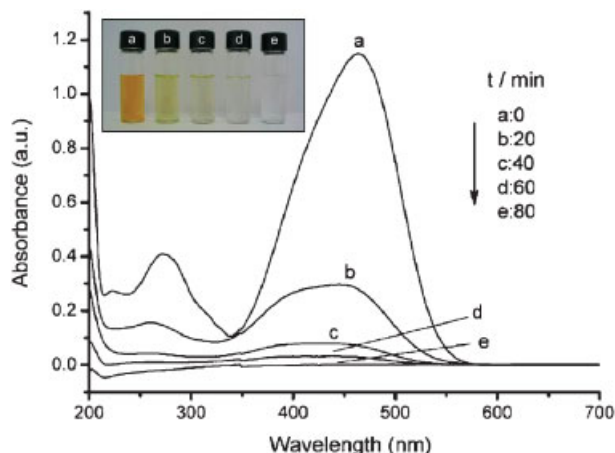
Figure 10. Time-dependent color change (see the photo in the upper inset) and corresponding time-dependent optical absorbance spectra for the MeOr solution (starting concentration: 5.0×10^{-5} M, 60 mL) in the presence of the micro/nanoarchitectured ZnO (30 mg) after its exposure to UV light for different durations.

Figure 11. The MeOr normalization concentration (from the optical absorbance measurements at 464 nm) in the solution (60 mL) with different catalysts (30 mg) versus the exposure time to UV light. Starting MeOr concentration C_0: 5.0×10^{-5} M. a) Without any catalyst, b) ZnO nanosheet powders, c) ZnO nanoparticle powders, d) ZnO nanoneedle powders, e) Degussa P25 titania powders, and f) the micro/nanoarchitectured ZnO.

The photocatalytic activity of the micro/nanostructured ZnO in the degradation of well-known organic azo-dye MeOr, a typical pollutant in the textile industry, was evaluated. Figure 10 shows the optical absorption spectra of a MeOr aqueous solution (initial concentration: 5.0×10^{-5} M, 60 mL) with 30 mg of the as-prepared ZnO powders shown in Figure 2 after exposure to ultraviolet light (UV) for different durations. The main absorption peak at 464 nm, which corresponds to the MeOr molecules, decreases rapidly with extension of the exposure time, and completely disappears after about 80 min. Further exposure leads to no absorption peak in the whole spectrum, which indicates the total decomposition of MeOr. A series of color changes in the sample is shown in the upper part of Figure 10, which corresponds to the sequential changes of the absorption measurements. It is clear that the intense orange color of the starting solution gradually disappears with increasing exposure time to the UV light.

To demonstrate the structure-induced enhancement of the photocatalytic performance of the micro/nanostructured ZnO, a further experiment was performed using other nanostructured ZnO powders (nanoneedles, nanosheets, and commercial nanoparticles, see Fig. S1 in the Supporting Information) and the commercial photocatalyst Degussa P25 titania. Thirty milligrams of the reference samples were added into identical MeOr solutions. The results are shown in Figure 11, which correspond to the MeOr normalization concentration in the solution versus the exposure time from the optical absorbance measurements at 464 nm. Without any catalyst, only a slow decrease in the concentration of MeOr was detected under UV irradiation (curve a in Fig. 11). The addition of catalysts leads to obvious degradation of MeOr, and the photocatalytic activity depends on the morphology. The activity increases in turn for the nanostructured ZnO powders: nanosheets (curve
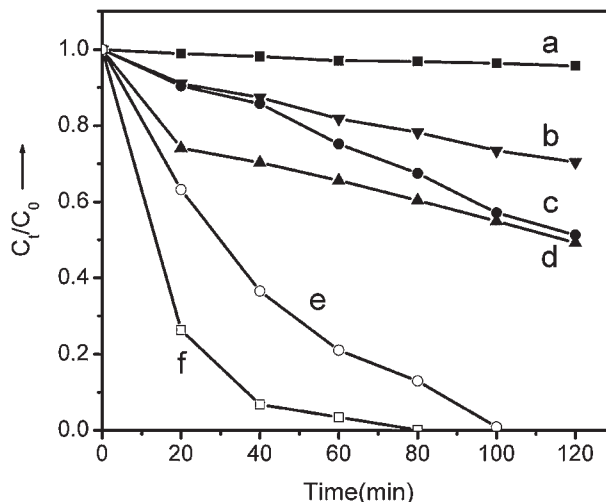
b), nanoparticles (curve c), and nanoneedles (curve d), but is still lower than that of the Degussa P25 titania (curve e). For the ZnO with a hierarchical micro/nanoarchitecture, however, the activity is much higher than that of the reference ZnO and even Degussa P25 (curve f). The MeOr solution is decolorized completely by using the micro/nanostructured ZnO after UV irradiation for 80 min.

The durability of photocatalytic activity was also studied by re-use of the catalysts in fresh MeOr under UV light irradiation. Figure 12 shows the photodegradation results for three cycles using the hierarchically micro/nanostructured ZnO, Degussa P25 titania, and ZnO nanoneedles (80 min irradiation for each cycle). The Degussa P25 titania exhibits the best durability and there is no significant change in the activity even after the third cycle. Comparatively, the
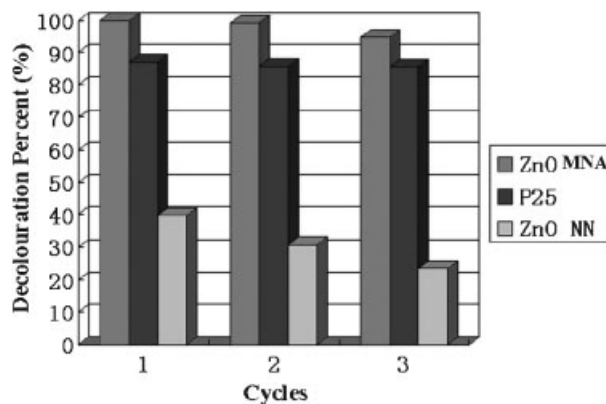

Figure 12. Comparison of photodegradation performance within three cycles (1: original, 2: first recycled, 3: second recycled) for the micro/nanoarchitectured ZnO (ZnO MNA), Degussa P25 titania (P25), and ZnO nanoneedles (ZnO NN), respectively.

hierarchically micro/nanostructured ZnO is more stable than the ZnO nanoneedles under UV irradiation. The decolorization percentage of the MeOr solution decreased from 100% to only 95% after three cycles.

The photocatalytic superiority of the hierarchically micro/nanostructured ZnO over the other nanostructured ZnO is easily understood. It can be attributed to their special structural features. The hierarchically micro/nanostructured ZnO possess a greater specific surface area ($\sim$185 $m^2 g^{-1}$) than the reference samples (Degussa P25 powders: $\sim$50 $m^2 g^{-1}$, and the commercial ZnO nanoparticles: $\sim$30.6 $m^2 g^{-1}$), which is obviously beneficial for the enhancement of photocatalytic performance. On the other hand, the vertical and net-like or grid-like arrangement of nanosheets, as well as the conic-shape of the ZnO micro/nanostructured objects, would effectively prevent aggregation and thus maintain a large active surface area. Comparatively, unwanted aggregation during the reaction usually leads to a significant decrease in the active surface area and thus the photocatalytic performance of the reference samples, such as Degussa P25 TiO_2 nanopowders.[19b,28] In addition, the unique structure of the hierarchically micro/nanostructured ZnO may increase the photocatalytic efficiency. The nanosheet thickness of 10 nm is close to the regime where quantum size effects are prominent. The nanosheets' bandgap broadening induced by quantum size effects would not only bring higher redox potentials, but also promote electrons transferring from the conductive bands of nanosheets with high electric-potential to those of the core-part micro-pyramid with low electric-potential. The probability of the photogenerated electron/hole pair recombination could then be reduced, which in turn enhances the charge-transfer rates in the materials.[19b] Thus a good photocatalytic performance is obtained. A more detailed and deeper understanding of the photocatalytic activity of the hierarchically micro/nanostructured ZnO is in progress.

As for the durability of the photocatalysts, since the experiments here were carried out in a nearly neutral solution (pH = 6.4 for the 5.0×10^{-5} M MeOr solution), the decrease in the photodegradation efficiency of the recycled ZnO catalysts can be attributed to photocorrosion rather than pH-dependent dissolution (chemical corrosion) of ZnO. Photocorrosion is a major obstacle for photocatalysts such as ZnO and CdS but not for TiO_2.[29] In this case, the hierarchically micro/nanostructured ZnO shows higher durability for photocatalytic activity than the ZnO nanoneedles, despite being lower than Degussa P25 titania, under UV light irradiation. The greater single-crystalline nature of the synthesized hierarchically micro/nanostructured ZnO would contribute to their good durability.[30]

Based on the results above, the advantages of such hierarchically micro/nanostructured ZnO as photocatalysts, compared with the other nanostructured ZnO powders (nanoparticles, nanoneedles, and nanosheets, etc.), are: 1) a high surface-to-volume ratio with effective prevention from further aggregation to maintain the high catalytic activity area arising from the grid-like structure. 2) Easier separation and

recycling than the common nanocrystals because of the larger size of the ZnO particles. 3) Higher redox potentials of the size-quantized nanosheets that stand on the micro-conic particles as a result of the increase in bandgap energy, which in turn enhances the charge-transfer rates in the system and reduces the non-radiation recombination of the electron-hole pair.

3. Conclusion

In summary, a novel ZnO hierarchical micro/nanoarchitecture with dense nanosheet-built networks that stand on hexagonal-pyramid-like microcrystals, which show a grid-like surface morphology, has been synthesized by a facile solvothermal procedure in the absence of self-assembled templates or matrixes. Because of its pyramid-like shape with grid-like structure, such ZnO particles have a high specific surface area and are stable against aggregation. The formation can be described by a two-step growth mode. A suitable release rate of Zn^{2+} ions into the reaction system (using Zn foil as a zinc source and controlling the ratio of V_{DIW}/V_{EDA} between 3:37 and 1:7) is requisite for the hierarchical growth of the micro/nanostructured ZnO. The special structural features of the micro/nanoarchitectured ZnO, i.e., a high surface-to-volume ratio with effective prevention from aggregation, leads to high photocatalytic activity, as observed in the decomposition of MeOr under UV light irradiation. Despite the lower durability than Degussa P25 titania, the micro/nanoarchitectured ZnO in this study could be a promising candidate for photocatalysis applications in some neutral solutions because of the facileness in separation, recycling, and mass production. In addition, this work provides an efficient route for the structure-induced enhancement of photo-catalytic performance. Such structure-induced enhancement could also be extended to the other catalysts, such as inherently excellent TiO_2, if they are of the same hierarchical micro/nanoarchitecture with open and porous nanostructured surface morphology.

4. Experimental

Preparation of Samples: All the chemicals were of analytic grade and used without further purification. In a typical procedure, a piece of zinc foil and NaOH (0.2 g) were added into an aqueous EDA solution (40 mL) with a V_{DIW}/V_{EDA} of 1:7 in a 50 mL Teflon-lined autoclave. The autoclave was then sealed and maintained at 160 °C for 12 h, followed by natural cooling to room temperature. Afterwards, the foil was taken out from solution, which was covered with product. It was subsequently rinsed with deionized water and absolute ethanol, and dried under vacuum ($\sim$10^{-3} torr) at 60 °C for 5 h.

Characterization: The final products on the Zn foil were characterized by X-ray diffraction (XRD, X'Pert Pro MPD), field emission scanning electron microscopy (FESEM, Sirion 200), and high-resolution electron microscopy (HRTEM, JEOL 2010). The nitrogen sorption isotherms were measured at −196.6 °C using a gas adsorption apparatus (model: BECKMAN SA3100 COULTER) for the samples. Specific surface areas were evaluated using the Brunauer–Emmett–Teller (BET) equation [21] and assuming the surface area occupied by one N_2 to be 0.162 nm^2.

Photocatalytic Activity Measurements: A cylindrical pyrex flask (capacity ~80 mL) was used as the photoreactor vessel. The reaction system that contained MeOr ($C_{14}H_{14}N_3SO_3Na$, 4-[[(4-dimethylamino)-phenyl]azo]benzenesulfonic acid sodium salt, Sigma–Aldrich Chemical Co) (5.0×10^{-5} M, 60 mL) and the as-synthesized product (30 mg), scraped off from the Zn foil, as catalyst, was magnetically stirred thoroughly in the dark to reach the adsorption equilibrium of the methyl orange on the catalyst before exposure to UV irradiation from a 60 W low-pressure Hg lamp (254 nm, 5 cm in distance from the flask). The pH value of the MeOr aqueous solution (5.0×10^{-5} M) was measured to be about 6.4. After different irradiation intervals, analytical samples were drawn from the photo reactor vessel and centrifuged. The centrifuged solution was sampled in a quartz cell with a 10 mm light path for optical absorbance measurement.

The optical absorption spectra were recorded on a Cary 5E UV-Vis-NIR spectrophotometer at room temperature. In addition to nanoneedle and nanosheet powders, which were also prepared in our laboratory, commercial ZnO nanoparticle powders (25–40 nm in size, Shanghai Chemical Reagent Co.) and TiO_2 nanopowders (25–30 nm in size, Degussa P25, Degussa Co.) were also adopted for reference catalysts to compare the photocatalytic activity under the same experimental conditions.

[1] K. Hara, *Sol. Energy Mater. Sol. Cells* **2000**, *64*, 115.

[2] G. Sberveglieri, S. Groppelli, P. Nelli, A. Tintinelli, G. Giunta, *Sens. Actuators B* **1995**, *25*, 588.

[3] J. A. Rodriguez, T. Jirsak, J. Dvorak, S. Sambasivan, D. Fischer, *J. Phys. Chem. B* **2000**, *104*, 319.

[4] H. Yumoto, T. Inoue, S. J. Li, T. Sako, K. Nishiyama, *Thin Solid Films* **1999**, *345*, 38.

[5] M. Monge, M. L. Kahn, A. Maisonnat, B. Chaudret, *Angew. Chem. Int. Ed.* **2003**, *42*, 5321.

[6] P. D. Yang, H. Q. Yan, S. Mao, R. Russo, J. Johnson, R. Saykally, N. Morris, J. Pham, R. R. He, H. J. Choi, *Adv. Funct. Mater.* **2002**, *12*, 323.

[7] Z. L. Wang, *J. Phys: Condens Matter* **2004**, *16*, R829.

[8] Z. L. Wang, X. Y. Kong, Y. Ding, P. X. Gao, W. L. Hughes, R. S. Yang, Y. Zhang, *Adv. Funct. Mater.* **2004**, *14*, 943.

[9] X. F. Gao, L. Jiang, *Nature* **2004**, *432*, 36.

[10] J. Y. Lao, J. G. Wen, Z. F. Ren, *Nano Lett.* **2002**, *2*, 1287.

[11] P. X. Gao, Z. L. Wang, *Appl. Phys. Lett.* **2004**, *84*, 2883.

[12] Y. G. Zhang, Z. Y. Wang, F. Lu, Y. Zhang, Y. H. Xiao, L. D. Zhang, *Appl. Phys. Lett.* **2006**, *89*, 113110.

[13] B. Liu, S. H. Yu, F. Zhang, L. J. Li, Q. Zhang, L. Ren, K. Jiang, *J. Phys. Chem. B* **2004**, *108*, 4338.

[14] C. L. Jiang, W. Q. Zhang, G. F. Zou, W. C. Yu, Y. T. Qian, *J. Phys. Chem. B* **2005**, *109*, 1361.

[15] S. Y. Yu, C. Wang, J. B. Yu, W. D. Shi, R. P. Deng, H. J. Zhang, *Nanotechnology* **2006**, *17*, 3607.

[16] T. R. Zhang, W. J. Dong, M. Keeter-Brewer, S. Konar, R. N. Njabon, Z. R. Tian, *J. Am. Chem. Soc.* **2006**, *128*, 10960.

[17] T. L. Sounart, J. Liu, J. A. Voigt, J. W. P. Hsu, E. D. Spoerke, Z. R. Tian, Y. B. Jiang, *Adv. Funct. Mater.* **2006**, *16*, 335.

[18] a) A. J. Hoffman, E. R. Carraway, M. R. Hoffmann, *Environ. Sci. Technol.* **1994**, *28*, 776. b) E. R. Carraway, A. J. Hoffman, M. R. Hoffmann, *Environ. Sci. Technol.* **1994**, *28*, 786.

[19] a) K. Sato, M. Aoki, R. Noyori, *Science* **1998**, *281*, 1646. b) C. H. Ye, Y. Bando, G. Z. Shen, D. Golberg, *J. Phys. Chem. B* **2006**, *110*, 15146.

[20] a) M. L. Curri, R. Comparelli, P. D. Cozzoli, G. Mascolo, A. Agostiano, *Mater. Sci. Eng. C* **2003**, *23*, 285. b) C. Hariharan, *Appl. Catal. A* **2006**, *304*, 55.

[21] S. Brunauer, P. H. Emmett, E. Teller, *J. Am. Chem. Soc.* **1938**, *60*, 309.

[22] S. C. Ma, in: *Basal Chemical Reactions*, Shaan'Xi Technology & Science Press, Xi'an, P.R. China **2003**, p. 377.

[23] X. D. Gao, X. M. Li, W. D. Yu, *J. Phys. Chem. B* **2005**, *109*, 1155.

[24] W. J. Li, E. W. Shi, W. Z. Zhong, Z. W. Yin, *J. Crystal Growth* **1999**, *203*, 186.

[25] a) G. Y. Zhang, X. Jiang, E. G. Wang, *Science* **2003**, *300*, 472. b) G. Y. Zhang, X. D. Bai, E. G. Wang, *Phys. Rev. B* **2005**, *71*, 113411.

[26] Z. Q. Li, Y. Ding, Y. J. Xiong, Q. Yang, Y. Xie, *Chem. Commun.* **2005**, 918.

[27] J. Y. Chen, T. Herricks, M. Geissler, Y. N. Xia, *J. Am. Chem. Soc.* **2004**, *126*, 10854.

[28] J. S. Hu, L. L. Ren, Y. G. Guo, H. P. Liang, A. M. Cao, L. J. Wan, C. L. Bai, *Angew. Chem. Int. Ed.* **2005**, *44*, 1269.

[29] a) V. van Dijken, A. H. Janssen, M. H. P. Smitsmans, D. Vanmaekelbergh, K. Meijerink, *Chem. Mater.* **1998**, *10*, 3513. b) B. Neppolian, H. C. Choi, S. Sakthivel, B. Arabindoo, V. Murugesan, *J. Haz. Mater.* **2002**, *89*, 303.

[30] H. L. Xu, W. Z. Wang, *Angew. Chem. Int. Ed.* **2007**, *46*, 1489.